Available online at www.sciencedirect.com
ScienceDirect
International Journal of Mass Spectrometry 269 (2008) 24–33
International Journal of Mass Spectrometry
www.elsevier.com/locate/ijms

Gas-phase ionisation of sputtered rare gas atoms

K. Wittmaack *

GSF – National Research Centre for Environment and Health, Institute of Radiation Protection, D-85758 Neuherberg, Germany

Received 1 August 2007; accepted 6 September 2007
Available online 19 September 2007

Abstract

During bombardment of solid samples with rare gas ions, charge-transfer events can convert reemitted rare gas atoms to positively charged ions. In analytical applications of secondary ion mass spectrometry (SIMS) this mechanism of ion formation is of considerable interest because, owing to their high ionisation potential, the ion fraction of sputtered rare gas atoms is very low. A quadrupole-based SIMS instrument was used to study details of the gas-phase ionisation process, notably the variation of the ion production rate as a function of the distance from the surface. The relevant information was derived from the apparent energy spectra of gas-phase generated (GPG) ions, observed during bombardment of a variety of elemental targets with Ne^+, Ar^+ and Kr^+ beams at energies between 3 and 12 keV. Owing to the use of a secondary ion extraction field of low strength, gas-phase ionisation events could be separated by distance δ from the surface, with δ up to about 6 mm. The results were compared with a simple model that describes the ion production rate as the product of the gas-atom flow rate and the ionisation probability. The first factor is proportional to the primary ion current and the second proportional to the current density j_0. Therefore, the intensity of GPG ions is not proportional to j_0^2, as assumed previously. The mean ionisation probabilities of GPG ions ($\sim 10^{-5}$ at a moderate mean current density of $\sim 2\,mA/cm^2$) were found to be higher by more than four orders of magnitude compared to 'ordinary' SIMS. In part, this favourable result can be attributed to the low energy of rare gas atom ejection (~ 0.1 eV). The experimental data suggest that the angular distributions of ejected rare gas atoms are strongly forward peaked. Presumably for this reason the yields of GPG ions observed with an amorphised target like silicon were distinctly higher than with polycrystalline metals. In the latter case, emission from unfavourably oriented microcrystals causes a large fraction of ejected gas atoms to escape from the interaction volume before ionisation can occur. Further enhancement in yield can be expected by the use of focussed primary ion beams with fairly uniform rather than Gaussian-like current density distributions. If the atomic number of the projectile is slightly lower than that of the target atom, as for Ne^+ impact on Mg, Al and Si or Ar^+ impact on Ti^+, sizable or even high signals, independent of current density, were observed due to energetic multiply scattered ions.

Keywords: Secondary ion mass spectrometry; Gas-phase ionisation; Charge transfer; Ionisation probability

1. Introduction

The mass spectrum of positive secondary ions generated by the impact of energetic (~ 10 keV) primary ions on solid targets has long been known [1,2] to contain a small fraction of species that were ejected from the sample not as ions but as neutrals, to become ionised only in vacuum (i.e., in the 'gas phase') at some sizable distance δ from the bombarded surface, well outside the region where ionisation and neutralisation is controlled by electronic interaction with the substrate. The distance δ may be assessed by making use of the fact that, to enhance the detection sensitivity in secondary ion (SI) mass spectrometers, an acceleration voltage $V_a = V_t - V_{ex}$ is commonly applied between the sample or target (at bias potential V_t) and an extraction electrode (V_{ex}) at a distance d from the sample surface. In the simple case of plane target and extraction electrodes arranged parallel to each other, the applied voltages establish a uniform electric field of strength $F_a = V_a/d$. If SIs of charge q are emitted from the sample surface with an initial kinetic energy E, their total energy E_Σ on arrival at the extraction electrode is

$$E_\Sigma = E + qV_a = E + qF_a d. \quad (1)$$

* Tel.: +49 89 3187 2439; fax: +49 89 3187 3323.
E-mail address: wittmaack@gsf.de.

1387-3806/$ – see front matter © 2007 Elsevier B.V. All rights reserved.
doi:10.1016/j.ijms.2007.09.006

If neutrals of energy E_g are ionised in the gas phase at a distance δ from the surface, their total energy $E_{\Sigma,g}$, becomes

$$E_{\Sigma,g} = E_g + qV_a\left(1 - \frac{\delta}{d}\right) = E_g + qF_a(d - \delta). \quad (2)$$

The energy $E^0_\Sigma = qV_{a,0} = qV_a(E = 0)$ at which SIs of kinetic energy $E = 0$ pass through the energy analyser defines a reference target bias $V_{t,0}$, as $V_{a,0} = V_{t,0} - V_{ex}$. Energy spectra of SIs are usually recorded as a function of V_t while keeping V_{ex} constant. Hence

$$E = q(V_{a,0} - V_a) = q(V_{t,0} - V_t). \quad (3)$$

According to Eq. (2) a gas-phase generated (GPG) ion will appear in the energy spectrum of secondary ions at a position that is shifted by the amount $-qV_a\delta/d = -qF_a\delta$ compared to the position E it would have if it had been ionised right at the surface. Hence GPG ions of very low energies will apparently feature 'negative' kinetic energies.

Two types of secondary ion mass spectrometers need to be distinguished. (1) In quadrupole-based instruments the acceleration voltage is usually low and the extraction gap comparatively large, typically $V_a = 100$ V and $d \approx 2$ cm (as in Atomika instruments), so that $F_a \approx 50$ V/cm (ignoring for the moment the effect of the screening electrode placed in front of the acceleration electrode). Assuming ionisation to takes place at $\delta = 200$ μm, a rather small shift of −1 eV is expected for singly charged ions. Published data are generally in accordance with this prediction in that the GPG ions exhibited narrow peaks close to zero-energy [3–5] (note that the exact position $E = 0$ is difficult to identify of the V_t scale). The observation of narrow peaks implies that the neutrals from which the ions were formed must have had rather low kinetic energies. (2) In magnetic sector field instruments, on the other hand, the acceleration voltage is high and the extraction gap small, so that the electric field strength F_a is very high. In Cameca IMS-3F instruments, for example, $V_{ex} = 0$, $V_{t,0} = 4.5$ kV and $d = 0.5$ cm, so that $F_a = 9$ keV/cm = 0.9 V/μm. For $0 < \delta < 200$ μm the expected shifts range between 0 and −180 eV. In support of this estimate, energy spectra of GPG ions [6–9] exhibited a peak near 0 eV, with a width depending on the band pass of the electrostatic analyser, and a long, almost exponential tail towards negative energies, extending to −100 eV and more. If the same species are also emitted as 'normal' secondary ions, the peak due to GPG ions is buried in the low-energy tail of the SIs [6,7,9].

Whereas the observation of ion signals at sizable 'negative' energies leaves little doubt that the ionisation process must have taken place at some distance from the surface, the actual mechanisms leading to ion formation are still not known in any detail. Ionisation by charge transfer between the primary ions and sputtered atoms or molecules has been invoked most often [1,4,6]. However, there is also the possibility that ionisation is due to the interaction of excited sputtered atoms [2,3]. Probably most surprising is the observation that gas-phase ionisation can also give rise to rather efficient production of doubly charged ions [1,2,4,6–8], and even triply charged ions like Te^{3+} and Hg^{3+} have been observed [7,10]. The total energy, ΣI, required to produce the latter ions (58.8 and 63.4 eV, respectively) is much larger than the ionisation potential I of the primary ion (for example, $I(O_2^+) = 14.0$ eV). Hence the interacting particles must have been in a highly excited, presumably metastable state.

From a practical point of view, gas-phase ionisation in secondary ion mass spectrometry (SIMS) is of particular interest when aiming at the analysis of rare gas elements which feature a high ionisation potential. As a result they are sputtered with very low ionisation probability (i.e., with a high 'relative sensitivity factor' [11]) because mechanisms like bond breaking [12,13] or electron tunnelling [14,15] do not work. Williams and Streit [8] pointed out that the successful SIMS analysis of He implanted in Si and GaAs under O_2^+ bombardment could hardly be understood other than by assuming that the authors [16] unknowingly recorded GPG He^+ ions. In support of this supposition, Ar and Kr implanted in semiconductors could be analysed with reasonable sensitivity using 5.5 keV O_2^+ bombardment to produce GPG ions [9].

Interest in gas-phase ionisation has recently been revived by the work of Desgranges and Pasquet [17] who reported on the SIMS analysis of Xe in UO_2. Rather surprising was the observation that the ionisation probability of GPG Xe^+ ions could be enhanced significantly by directing a jet of oxygen gas at the sample sputtered by 10 keV O_2^+ ions. The mechanism of this yield enhancement effect has not been identified in detail yet.

The purpose of this study was a detailed evaluation of gas-phase ionisation phenomena observed during bombardment of a variety of elemental targets with different rare gas ions (Ne, Ar and Kr). Possible impact-energy dependent effects were explored by covering energies between 3 and 12 keV.

2. Experimental

The experiments were performed using the quadrupole-based DORAMIS secondary ion mass spectrometer described elsewhere [5]. Briefly, rare gas ions were produced in a plasma ion source, either filament-assisted or cold-cathode type. The primary ion beam was mass analysed using a 30° magnetic sector field. The achieved mass resolution m/Δ was about 100, sufficient to resolve the isotopes of a Kr^+ ion beam. Ion bombardment was performed with a focussed beam raster scanned over a square with a side length of typically two to three beam diameters. The impact angle θ_0 was 2° to the surface normal. Secondary ions released from or generated in front of the ion-bombarded target were transported through a simple parallel-plate electrostatic analyser, biased to extraction voltages between typically −50 and −200 V. The target bias could be varied between −100 and +100 V. Following energy analysis, the secondary ions were retarded to energies of about 10 eV, appropriate for achieving good mass resolution in the quadrupole analyser [18]. During the experiments the total pressure in the analysis chamber was less than 5×10^{-9} hPa.

Polycrystalline metal samples of Mg, Al, Ti, Cu and Ag, with >99.99% purity, about 1 mm thick and ca. 6 × 10 mm wide, served as targets. A thin Al foil cut from a standard household roll was used for comparison. Silicon samples, n-type, were cut from commercial wafers.

3. Results

The essential spectral features of GPG Ar^+ ions, as observed in DORAMIS, are illustrated in Fig. 1. The results relate to Ar^+ bombardment of Si and measurements at $V_{ex} = -50$ V. The energy spectrum of Si^+ secondary ions is shown for comparison. The prominent peak due to GPG Ar^+ ions is centred at secondary ion energies near zero and exhibits a left-hand tail that extends significantly into the region of 'negative' energies. GPG Ar^{2+} ions were also observed with sizable intensity. The Ar^{2+}/Ar^+ peak intensity ratio was roughly 2%. A similar ratio has previously been observed in GPG spectra of Ar^+ bombarded GaAs [19]. This ratio may tentatively be interpreted as the fraction of Ar atoms that left the sample in an excited state, carrying sufficient internal energy for double ionisation in a charge-transfer event.

The origin of the energy scale, and hence the actual position of the Ar^+ peak, is subject to an estimated uncertainty $e\Delta V_{t,0} = \pm 1$–2 eV. The peak width is determined by the band pass w of the energy filter and the shift in the apparent energy due to ionisation at distance δ. Width and shift are expected to increase with increasing acceleration voltage. To explore the V_a-dependence, Fig. 2 shows Ar^+ spectra for three different extraction voltages, ranging from -50 to -150 V. To ease comparison, the target bias is shown on a reduced scale, $(V_{t,0} - V_t)/w_{0.5}$, where $w_{0.5}$ is the full width at half-maximum (FWHM) of the Ar^+ peak. Within experimental uncertainty, the Ar^+ peaks are seen to have identical shapes on the reduced V_t scale. The measured peak widths are shown in the inset of Fig. 2 versus the applied extraction voltage (solid diamonds). Within experimental accuracy $w_{0.5}$ is directly proportional to V_a.

Interpretation in terms of a very low kinetic energy of the GPG Ar^+ ions is supported by previously reported velocity distributions of Ar atoms released from Ar bombarded Si (3 keV, 60° to the surface normal) [20]. Measured time-of-flight (TOF) spectra recorded at target temperatures T_{targ} between 80 and 290 K could be fitted by two Maxwell–Boltzmann (MB) distributions, one corresponding to outdiffusing Ar atoms ($T_{MB,o} = T_{targ}$), the other, comprising about 60% of the total signal, to Ar atoms

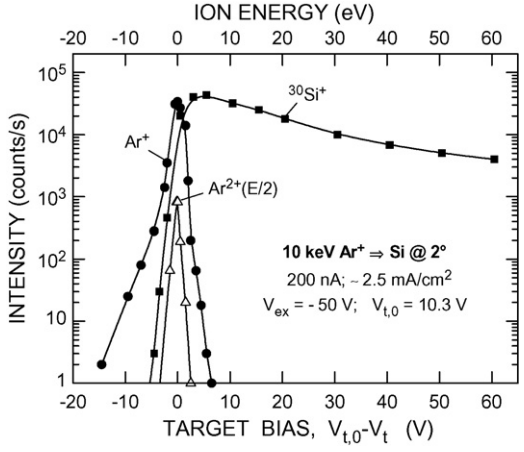

Fig. 1. Energy spectra of different ions generated during Ar^+ bombardment of Si.

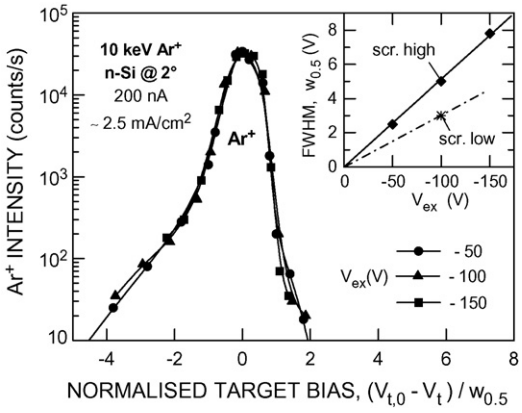

Fig. 2. Comparison of the energy spectra of GPG Ar^+ ions recorded at different extraction voltages. The target bias is presented on a reduced scale. The inset shows the full width at half-maximum of the distributions versus the extraction voltage.

contained in exploding Ar bubbles which were assumed to have been formed during continuous Ar implantation in the amorphised Si sample ($T_{MB,b}$ between 1650 and 1850 K, corresponding to mean kinetic energies between 0.14 and 0.17 eV). At implantation energies between 10 and 150 keV, evidence for bombardment-induced rare gas outdiffusion [21], bubble formation [22,23] and bubble rupture (blistering) [22] has been obtained using Rutherford backscattering spectrometry (RBS). Details of blister shape were identified by scanning electron microscopy [22].

It should be mentioned that, at a given extraction voltage, the width of the GPG ion peaks depended of the voltage, V_{sc}, applied to the screening electrode which is located in front of the extraction electrode [24]. Typically $0.1 \leq V_{sc}/V_{ex} \leq 0.3$. The screening electrode covers a large fraction of the extraction electrode so that the actual electric field strength in the vicinity of the target is distinctly lower than V_a/d, as shown in detail by numerical field simulations [19]. In standard SIMS measurements the extraction electrode serves the purpose of improving secondary ion transport through the energy filter [24]. The results of Fig. 2 were obtained with a 'high' ratio V_{sc}/V_{ex}. The asterisk in the inset of Fig. 2 shows an example for measurements performed with a 'low' ratio V_{sc}/V_{ex}.

Energy spectra of Ar^+ ions observed during Ar bombardment of a Ti target are presented in Fig. 3 for two different current densities but the same beam current, using either a focussed or a slightly defocussed beam. Several observations are noteworthy. (i) The peak intensity of the GPG Ar^+ ions decreased with decreasing current density. (ii) By contrast, the intensity in the 'negative'-energy tails of the GPG Ar^+ spectrum was essentially independent of the current density. (iii) In addition to the narrow GPG Ar^+ peak, the Ar^+(Ti) spectrum revealed pronounced signals in the region of positive secondary ion energies. These Ar^+ ions are attributed to multiply scattered projectiles [5] which experienced sufficiently close collisions with Ti target atoms to generate, by electron promotion [25], an $M_{2,3}$ vacancy in the scattered Ar atom. Some additional excitation of outer-shell electrons is likely to have occurred as well. Scattered Ar atoms

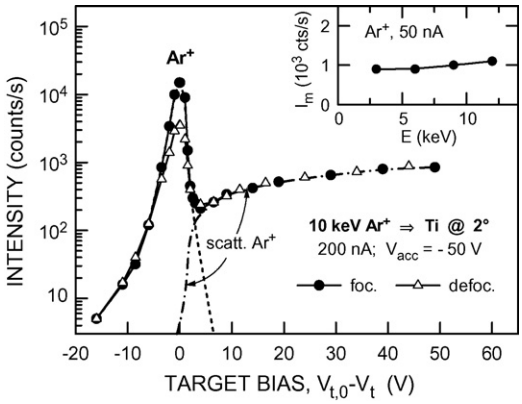

Fig. 3. Energy spectra of Ar^+ ions observed during bombardment of Ti with either a focussed or a defocussed Ar^+ ion beam of the same current. The beam diameters were approximately 100 and 300 μm. The tentative separation into GPG and scattered ion distributions is denoted by dashed and dash-dotted lines. The inset shows the peak Ar^+ intensities versus the beam energy.

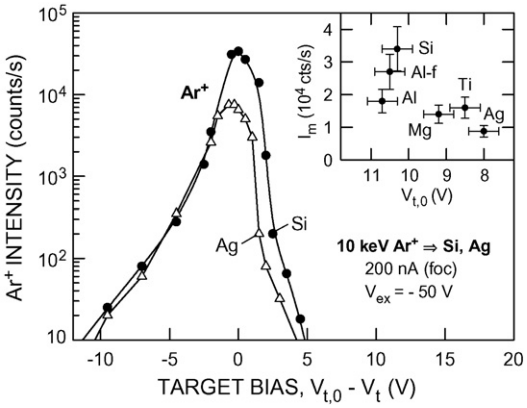

Fig. 4. Comparison of the GPG Ar^+ energy spectra observed during bombardment of Si and Ag. The inset shows peak Ar^+ intensities for different target materials versus the target bias corresponding to secondary ions of energy $E = 0$. Al-f denotes the result for an aluminium foil.

excited close to the surface will have a chance to escape from the Ti target into vacuum where ionisation takes place subsequent to Auger deexcitation. Inner shell excitation of Ar in Ar–Ti collisions is possible because the excitation occurs preferentially in the atom with the lower atomic number [26]. Compared to Ti, the probability for Ar excitation in Ar–Si collisions is lower by several orders of magnitude, at least for L-shell excitation below 15 keV [26]. Hence it is not surprising that Ar^+ signals due to multiply scattered Ar atoms in Si were not observed in the experiments of Fig. 1. (iv) As one might have expected, the ion formation efficiency due to $M_{2,3}$ vacancy formation in Ar/Ti was found to be independent of the primary ion current density: for $V_{t,0} - V_t > 5$ V, the data in Fig. 3 denoted by solid circles and open triangles fall on the same line. The estimated contributions of GPG and scattered Ar^+ ions to the total signal in the region of slightly positive secondary ion energies are denoted by dashed and dash-dotted lines.

The inset of Fig. 3 depicts the primary ion energy dependence of the peak intensity, I_m, of GPG Ar^+ ions observed for Ar^+ impact on Ti. A comparatively low current of 50 nA was used in order to produce focussed spots with sizes largely independent of the beam energy. Under these conditions I_m was found to be almost independent of the beam energy. The very small increase with increasing energy suggests that a minor decrease in spot size with increasing energy could have occurred. Corrected for spot size, I_m might even decrease slightly with increasing beam energy, as one would expect from the energy dependence of the cross section for charge transfer (20% decrease in going from 3 to 9 keV [27]).

A comparison of $I_m(Ar^+)$ in the spectra of Figs. 1 and 3 reveals sizable differences. Further studies revealed a dependence of the peak shape and the peak intensity on the target material. However, as the results of Fig. 4 show, the 'negative'-energy tails of the Ar^+ peaks are largely independent of the target material. According to the data presented in the inset, the peak intensities are somehow associated with $V_{t,0}$: targets with high I_m feature high $V_{t,0}$. Attempts to attribute this variation of $V_{t,0}$ to differences in the work function Φ of the target failed: Al, Ti and Ag, which cover the full spectrum of $V_{t,0}$ values in the inset of Fig. 4, feature essentially the same work function, $\Phi = 4.3$ eV [28].

The characteristic features of gas-phase ionisation described for Ar^+ primary ions were observed with other inert gas ions as well. Examples for Ne^+ impact on Al and Ti are presented in Fig. 5. The measurements were performed with a standard setting of the screening voltage (low) so that the energy resolution was distinctly better than for the data of Figs. 1–4 (see above). Compared to Figs. 1 and 3, the most important difference is that high Ne^+ signals due to scattered ions were observed with the Al target, for the same reasons as outlined with reference to the case Ar^+/Ti: Ne has a lower atomic number than Al and, hence, inner shell vacancies may be produced efficiently by electron promotion. In the case of Ne^+/Ti, on the other hand, electron promotion is very inefficient due to the pronounced mismatch in atomic numbers (and electronic levels).

A rather interesting aspect of the results in Fig. 5 is the observation of a significant plateau in the 'negative'-energy section of the Al^+ spectrum. Another example for Mg^+ emitted from Ne^+ bombarded Mg is shown in Fig. 6. As the target bias $V_{t,0} - V_t$ was reduced below the value corresponding to the peak of the Mg^+ secondary ion energy distribution, the ion intensity decreased rapidly by more than four orders of magnitude, passed

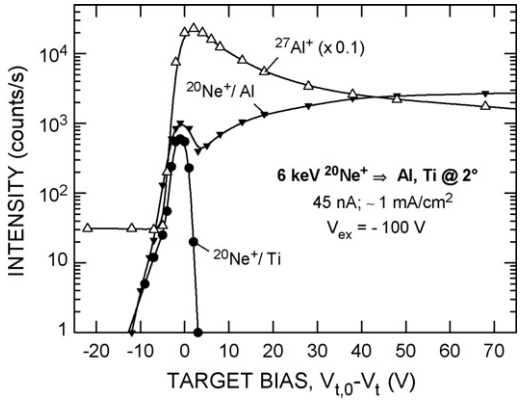

Fig. 5. Energy spectra of different ions generated during 6 keV Ne^+ bombardment of Al and Ti.

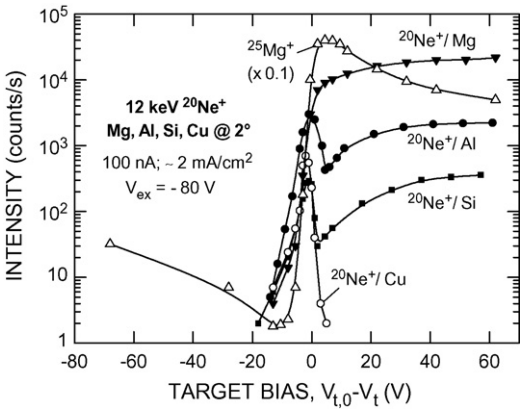

Fig. 6. Energy spectra of different ions generated during 12 keV Ne^+ bombardment of Mg, Al, Si and Cu.

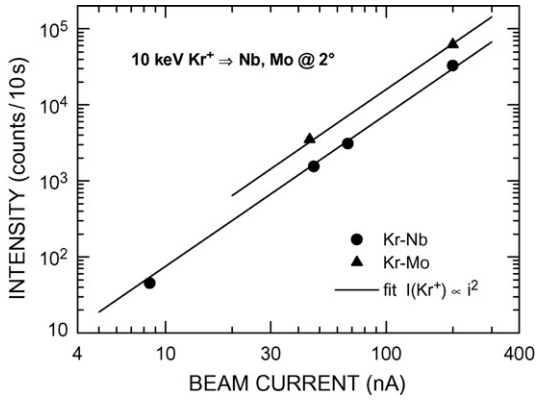

Fig. 7. Dependence of the GPG Kr^+ peak intensity on the beam current observed during bombardment of Nb and Mo targets with isotopically pure Kr^+ beams of nominally the same beam size and shape.

though a minimum and then increased. The spectral details in this region depended somewhat on the setting of the energy analyser. Results similar to those for Mg^+ from Ne^+ bombarded Mg were observed for Ti^+ from Ar^+ bombarded Ti (not shown). 'Negative'-energy tails are also present in a variety of spectra of singly charged ions reported by Schauer and Williams [29] for 8.5 keV Ar^+ impact on metals of the third and fourth row of the periodic system. However, a minimum as in the Mg^+ spectrum of Fig. 6 was not present in the previous data. This could be due to the fact that the previous study was performed with a magnetic sector field instrument.

The spectra of GPG and scattered Ne^+ ions in Fig. 6, for targets of Mg, Al, Si, and Cu, confirm the trends discussed above. High yields of scattered Ne^+ were observed with the light-element targets, but not with Cu. The GPG Ne^+ peak for Al is quite broad and much more intense than the peaks for Si and Cu. Owing to the very high signal due to Ne^+ scattered from Mg, the GPG Ne^+ peak appears to be hidden in the low-energy tail of the scattered ion signal. Note the interesting observation that the scattered Ne^+ intensity increases in the order Si–Al–Mg, i.e., the intensity is higher the more symmetrical the projectile–target atom collisions.

To study the yields of GPG as a function of the beam current i_0 or the current density j_0, one has to vary the beam current without changing the spot size and the spot shape. With the instrument used in the present study, this could be accomplished most conveniently with an inert gas featuring several isotopes of different abundance and by operating at sufficiently low maximum beam currents so that space charge expansion could be avoided. The most suitable inert gas species is Kr which, for the purpose in question, features useful isotopes with abundances γ between 2.25% (^{80}Kr) and 57% (^{84}Kr). Keeping the operating parameters of the ion source fixed, the beam currents $i_{0,\beta}$ of the different isotopes varied as expected, i.e., $i_{0,\beta} = \gamma\, i_0$. Measurement of GPG Kr^+ ions, observed during 10 keV Kr^+ bombardment of Nb and Mo, were performed with $i_0 = 390 \pm 10$ nA (except for $^{86}Kr^+$, in which case the beam current was set to 200 nA). The experimentally observed dependence of $I_m(Kr^+)$ on $i_{0,\beta}$ is presented in Fig. 7. The width of the GPG Kr^+ peaks was found to be rather large, 9 eV for Nb and 11 eV for Mo ($V_{acc} = -100$ V). The peak intensities are in accordance with a relation of the form $I_m \propto i_0^2$, represented by the two straight lines. However, due to the fixed beam size, relations of the form $I_m \propto j_0^2$ and $I_m \propto i_0 j_0$ would also be in accordance with the measured data.

4. Discussion

The results presented in the preceding section suggest that the phenomenon of gas-phase ionisation of inert gases released from inert gas bombarded solids can be described in terms of a simple charge transfer process. Electronic excitation of the released atoms does not seem to be a necessary requirement for ionising the reemitted atoms. This statement is based on the observation that the yields of GPG ions were generally not enhanced if the chosen projectile–target combination favoured projectile excitation, as in the case of bombardment of Al and Si with Ne^+ or of Ti with Ar^+. The lack of a correlation between excitation and gas-phase ionisation is understandable considering the fact that, under the conditions of this study, both processes are of low probability (usually $<10^{-5}$, see below), so that the product of the two probabilities becomes very low.

To discuss the present results in quantitative terms, we make recourse to the formalism used to describe ionisation of a gas of atoms (or molecules) of density n (cm^{-3}) by impact of electrons and ions [30]. The ion production rate $\dot{N}^+$ (ions/s) is related to the charge-transfer cross section σ (cm^2) and an effective interaction length L (cm) as

$$\dot{N}^+ = \frac{\sigma n L i_0}{e} = \sigma n L \nu_0, \tag{4}$$

where $\nu_0 = i_0/e$ (ions/s) is the primary ion flux. The length L is usually not known very well, but previous results were found to be in accordance with reasonable assumptions [30].

In the present study ion bombardment and gas-phase ionisation was carried out with a focussed, rotationally symmetric beam. Such beams can be described reasonably well by a Gaussian-like flux density distribution, $\varphi(\rho) = \varphi_0 \exp(-\rho^2/{\rho_0}^2)$, where ρ is the distance from the beam axis and φ_0 (cm^{-2} s^{-1}) the peak flux density [31]. The beam size ρ_0 was chosen so as to represent an 'effective radius' which connects flux and flux den-

sity in the simple form $\nu_0 = A\varphi_0 = \pi\rho_0^2\varphi_0$, where $A = \pi\rho_0^2$ is an 'effective' area of bombardment. The product $V = LA$ defines an 'effective' interaction volume. Using these parameters, Eq. (4) reads

$$\dot{N}^+ = \sigma n L A \varphi_0. \tag{5}$$

The interaction volume contains $N = nLA$ atoms which, during time τ, will be exposed to a mean primary ion fluence $\varphi_0\tau$ (cm^{-2}). The total number, N^+, of generated ions and the corresponding ionisation probability α^+ are

$$N^+ = \dot{N}^+\tau = \sigma N \varphi_0 \tau \tag{6}$$

and

$$\alpha^+ = \frac{N^+}{N} = \sigma\varphi_0\tau. \tag{7}$$

If the gas could be confined to the volume V, and in the absence of losses, complete ionisation, i.e., $\alpha^+ = 1$, could be obtained by exposure to a fluence $\varphi_0\tau = 1/\sigma$. The symmetric charge-exchange cross sections for $Ar^+ + Ar \rightarrow Ar + Ar^+$ range from $2.5 \times 10^{-15}\,\mathrm{cm}^2$ at 1.5 keV to $1.7 \times 10^{-15}\,\mathrm{cm}^2$ at 10 keV [27]. Hence fluences between 4 and $6 \times 10^{14}\,\mathrm{cm}^{-2}$ would suffice to achieve the hypothetical state of complete ionisation. In any case it is important to note that charge-exchange ionisation is a very efficient process.

Considering now the ionisation of inert gases reemitted from a solid bombarded with a beam of inert gas ions, the question is which meaning one should assign to the parameters n and L in Eqs. (4) and (5). To discuss the issue, the following parameters need to be defined: the polar angle, θ, of atom emission with respect to the surface normal; the radial distance, r_i, from the beam axis at which an atom is emitted, the radial distance, $r - r_\mathrm{i}$, of the departing atom from the surface normal through the point of emission, the distance, z, from the surface parallel to the surface normal, and the total distance, R, travelled by the atom, where $R^2 = z^2 + (r - r_\mathrm{i})^2$. With $\psi_\mathrm{s} = \psi_\mathrm{s}(z, r, \theta)$ denoting the angular distribution of ejected (sputtered) gas atoms, the flux density at distance R is $\psi_\mathrm{s} = \nu_0\psi_\mathrm{s}/R^2$. If these particles intersect the interaction volume with velocity υ_s, the equivalent particle density n_s in that volume is

$$n_\mathrm{s}(z, r, \theta) = \frac{\Psi_\mathrm{s}}{\upsilon_\mathrm{r}} = \frac{\nu_0\psi_\mathrm{s}}{\upsilon_\mathrm{s}R^2}. \tag{8}$$

Inserting Eq. (8) in Eq. (5) we have

$$\dot{N}_\mathrm{s}^+ = \sigma\varphi_0\nu_0\frac{LA\psi_\mathrm{s}}{\upsilon_\mathrm{s}R^2}. \tag{9}$$

The angular distribution of the ejected atoms is assumed to feature radial symmetry, being of the simple form

$$\psi_\mathrm{s} \equiv \psi_\mathrm{s}(\theta) = \frac{m+i}{2\pi}\cos^m\theta. \tag{10}$$

The normalisation factor ensures that the integral over all angles θ is unity. At distances much larger than the beam diameter D, i.e., for $R \gg D$, the ion production rate becomes

$$\dot{N}_\mathrm{s}^+ = \left(\frac{\sigma\varphi_0 L}{\upsilon_\mathrm{s}}\right)\frac{m+1}{2\pi R^2}A\nu_0\cos^m\theta. \tag{11}$$

The term in parentheses defines the ionisation probability of the process,

$$\alpha^+ = \frac{\sigma\varphi_0 L}{\upsilon_\mathrm{s}}. \tag{12}$$

The second term in Eq. (11) represents the flow rate $\dot{N}_\mathrm{s}$ of sputtered particles into angle θ through the area A covered by the ionising beam,

$$\dot{N}_\mathrm{s}(R, \theta) = \frac{m+1}{2\pi R^2}A\nu_0\cos^m\theta. \tag{13}$$

Written in the form of Eq. (11) it becomes evident that the ion production rate, and hence the measured ion signal, is proportional to the product $\nu_0\varphi_0$, i.e., neither proportional to φ_0^2 nor to ν_0^2. This is due to the fact that the number of atoms available for ionisation in the interaction volume is proportional to ν_0, see Eq. (13), but their ionisation probability is proportional to φ_0, see Eq. (12).

The analogy of Eq. (12) to Eq. (7) becomes evident by realising that $L/\upsilon_\mathrm{s} = \tau_\mathrm{s}$ is the time it takes for the ejected particle to travel fully through the interaction volume of length L. In that sense the ionisation probability is not a constant but dependent on the properties of the ejected particles, specified by their velocity υ_s. The interaction length is an instrumental parameter and can interpreted as the distance $\delta(w_\mathrm{i}) \equiv L$ that corresponds to the intrinsic energy resolution, $\Delta E_\mathrm{i} = ew_\mathrm{i}$, of the energy filter, which is that fraction of the apparent band pass that does not contain the broadening due to the energy shift caused by gas-phase ionisation. To assess L we assume, with reference to the results of [20], that the inert gas atoms were ejected with negligible energy, i.e., $E \ll \Delta E_\mathrm{i}$. The balance of target voltages $V_{\mathrm{t},0}(\delta = 0) = V_{\mathrm{t},0}^0$ and $V_{\mathrm{t},0}(\delta) = V_{\mathrm{t},0}^\delta$ required to transport zero-energy GPG ions through the energy analyser reads

$$(V_{\mathrm{t},0}^\delta - \beta V_\mathrm{ex})\left(1 - \frac{\delta}{d}\right) = V_{\mathrm{t},0}^0 - \beta V_\mathrm{ex}. \tag{14}$$

The factor $\beta < 1$ describes the effective lowering of the extraction field in the vicinity of the target due to the presence of the screening electrode. Rearrangement of Eq. (14) yields

$$\delta/d = \frac{V_{\mathrm{t},0}^\delta - V_{\mathrm{t},0}^0}{V_{\mathrm{t},0}^\delta - \beta V_\mathrm{ex}}. \tag{15}$$

With $V_{\mathrm{t},0}^{\delta=L} - V_{\mathrm{t},0}^0 \equiv w_\mathrm{i}$ the interaction length near the surface becomes

$$L \equiv \delta(w_\mathrm{i}) = \frac{w_\mathrm{i}d}{V_{\mathrm{t},0}^0 - \beta V_\mathrm{ex}}, \tag{16}$$

where the small difference between $V_{\mathrm{t},0}^\delta = V_{\mathrm{t},0}^0 + w_\mathrm{i}$ and $V_{\mathrm{t},0}^0$ is ignored.

The energy resolution increases linearly with increasing acceleration voltage. Hence L will change only slightly over

the narrow range of target voltages scanned to record an energy spectrum. Previously reported secondary ion energy spectra [4] suggest that the intrinsic energy resolution is about 1 eV at an extraction voltage of 100 V; hence $w_i = 10^{-2}|V_{ex}|$. With a typical value of $V^0_{t,0} = 10$ V, $V_{ex} = -100$ V, $d = 2$ cm and assuming $\beta = 0.3$, one finds $L = 0.05$ cm. With $\sigma = 1.7 \times 10^{-15}$ cm^2 at 10 keV [31], $\varphi_0 = 1.6 \times 10^{16}$ cm^{-2}s^{-1} (2.5 mA/cm^2) and $v_s = 1 \times 10^5$cm/s (0.2 eV Ar [20]) we find $\alpha^+ = 1.4 \times 10^{-5}$. This number is much higher than expected in 'ordinary' secondary ion emission of inert gases. The relative sensitivity factors for rare gas analysis by SIMS, reported by Wilson and Novak [11], are likely not to be representative of secondary ions but rather of GPG ions. Measurements of ionisation probabilities of rare gas secondary ions, α^+_{SI}, were not the topic of this work. However, the absence of a detectable Ar^+ signal at energies above about 5 eV in Fig. 1 implies that the probability of Ar^+ secondary ion ejection was lower by more than four orders of magnitude than the probability of ion formation in a charge-transfer process. Hence, $\alpha^+_{SI}(Ar) < 10^{-9}$.

The evaluation presented above may finally be extended to considering gas-phase ion production as a function of the distance δ from the surface. The results of the conversion of apparent energy spectra to ion signals as a function of distance δ according to Eq. (15) are presented in Fig. 8 for Ar bombardment of Si, Ti and Ag. Most of the data were obtained at an extraction voltage of −50 V; results obtained for Si at $V_{ex} = -100$ and −150 V are also shown. In all cases the GPG Ar^+ signals recorded at distances of ionisation up to 400–600 μm are seen to be constant within experimental accuracy, but different for the three target materials investigated. At larger distances the signals decrease, first slowly and then more rapidly. The results suggest a maximum distance of ion detection somewhere around 7–8 mm. This is a rather reasonable result because the quoted distance corresponds to the crossing point of the primary ion beam axis with the tangent to the ion trajectory at the entrance of the energy analyser [24].

For a detailed comparison of measured and calculated gas-phase ionisation data we make use of the fact that, for an impact angle close to normal ($\theta_0 = 2°$) as in this work, we can set $R = \delta$. Hence, with $A = \pi\rho_0^2$, the ion production rate in Eq. (11) simplifies to

$$\dot{N}^+_s = 0.5\alpha^+(m+1)\left(\frac{\rho_0}{\delta}\right)^2 \nu_0 \langle \cos^m\theta \rangle . \quad (17)$$

The factor $\langle \cos^m \theta \rangle$ represents the mean of the cosine factor, averaged overall interaction lengths contributing to ionisation. In the case of polycrystalline samples one also needs to take a proper average over the different orientations of the microcrystals.

At distances $0.5 < \delta < 2$ mm, the fall-off of the Ar^+ signal in Fig. 8 is roughly in accordance with the z-dependence predicted by Eq. (17), as indicated by the dash-dotted line. Hence it would be tempting to evaluate ion production rates in quantitative terms. The problem is that we have no a-priori knowledge of the exponent m. If implanted gas atoms are transported to and released from the surface by diffusion (rather than being ejected after having received a sizable amount of momentum and kinetic energy in the collision cascade), they would be expected to be emitted preferentially in the direction of the surface normal. If ejection occurs as a result of blistering, the angular distribution is likely to be still forward peaked, but probably broader than in the case of outdiffusion. A pronounced forward emission characteristics may be inferred from the time-of-flight study of van Veen et al. [20] already mentioned above. The authors measured the velocity distribution of Ar reemitted along the surface normal of Ar bombarded Si. After a flight path as long as 37 cm, the atoms were detected in a commercial residual-gas analyser composed of an electron-impact ioniser, a quadrupole mass filter and an electron multiplier [32]. The expected signal I^+ (counts/s) can be written

$$I^+_{TOF}(\theta = 0) = \eta_{RG}\varepsilon_{TOF}\frac{m+i}{2\pi R^2} A_{RG} A_0 \varphi_0, \quad (18)$$

where η_{RG} is the total ionisation and detection efficiency of the residual gas analyser, ε_{TOF} the effective duty cycle of the time-of-flight system, and A_{RG} is the entrance aperture of the residual gas analyser. With $\varphi_0 = 5 \times 10^{14}$ ions/cm^2 s [20], an assumed bombarded $A_0 = 10^{-2}$ cm^2 (corresponding to a beam current $i_0 = e\varphi_0 A = 0.8$ μA), $R = 37$ cm, a typical sensitivity $\eta_{RG} = 10^{-8}$ [33], and $\varepsilon_{TOF} = 0.25$ [32] one finds $I^+ = 1.5(m+1)$ s^{-1}. Noting further that the velocity distribution was allocated into about 50 channels, it is difficult to see how a statistically significant experiment could have been performed other than by assuming that m was quite large. Hence $m = 10$ may be a reasonable choice for Ar bombarded Si.

We use this estimate and the ionisation probability quoted above. Furthermore, we set $\delta = 1$ mm, $\rho_0 = 50$ μm, $\nu_0 = 1.3 \times 10^{12}$s^{-1} ($i_0 = 200$ nA) and $\langle \cos^m \theta \rangle = 0.8$ to find $\dot{N}^+_s = 2 \times 10^5$ s^{-1}. This number is a factor of about 30 larger than the experimental result for Si in Fig. 8, implying that the total detection and transmission efficiency of the mass spectrometer was about 3%. An efficiency of 5% was previously derived from experiments in which Ar gas bled into the sample chamber was ionised by Ar impact [30]. The estimated efficiency was considered high for a quadrupole-based system. The favourable result was attributed to the low kinetic energy of the ionised atoms, an argument that applies in this case as well. On a conservative side one may conclude that the results of the two studies are consis-

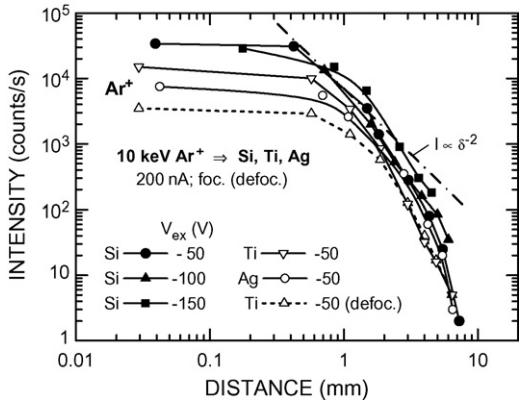

Fig. 8. The results of Figs. 1–4 converted to a presentation of ion yields versus the distance of ion formation from the surface.

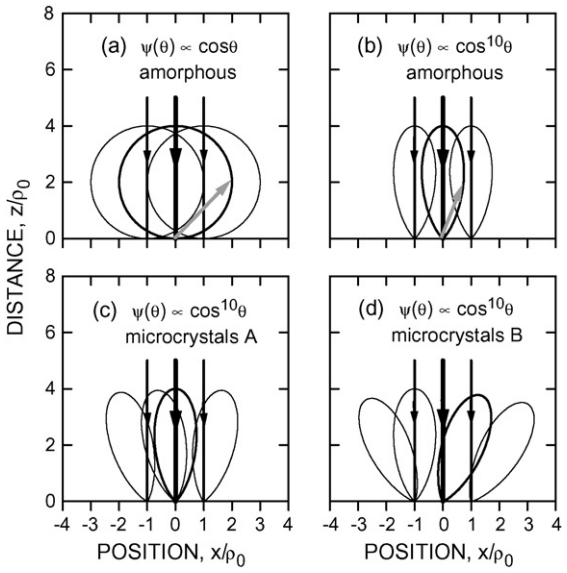

Fig. 9. Schematic illustration of broad and narrow angular distributions of sputtered atoms, for amorphous and polycrystalline targets.

tent with a low-energy transmission and detection efficiency on the order of 1%.

For a more general discussion of the results of Fig. 8 it is helpful to consider the different situations that one may encounter in gas-phase ionisation, as illustrated schematically in Fig. 9. The black arrows denote the incident beam; the outermost arrows define the full width at half-maximum. Panel (a) depicts cosine distributions of emission ($m = 1$), panel (b) shows the case of strongly forward peaked distributions with $m = 10$. The distributions in Fig. 9(a) and (b) relate to an amorphous target. The grey arrows denote atoms emitted in the directions corresponding to the 50% level of the maximum flux density. The large difference between $m = 1$ and 10 is evident. In the case $m = 1$ a very large fraction of the emitted atoms will escape from the interaction volume after having travelled only a short distance away from the surface, thus having essentially no chance to becoming ionised. Panels (c) and (d) of Fig. 9 illustrate conceivable angular distributions for a target composed of differently oriented microcrystals, assuming $m = 10$. It is clear that the gas atoms ejected from microcrystals with their surface normal pointing strongly away from the macroscopic surface normal will also be very prone to escape without getting ionised. Hence even though the emission cones for atoms released from a microcrystal may be very narrow, equivalent to $m = 10$, the mean angular distribution will correspond to a much smaller m-value.

One of the interesting results of Fig. 8 is the observation that the Ar^+ signal, recorded at distances $\delta \geq 2$ mm during Ar bombardment of Ti, remained the same when changing the beam size while keeping the beam current constant. This result is fully in accordance with the predictions of Eq. (11). If one keeps ν_0 constant but increases ρ_0 moderately, $\dot{N}_s^+$ remains constant because $\dot{N}_s$ increases proportional to $A = \pi\rho_0^2$, whereas α^+ decreases with increasing A as $\varphi_0 = \nu_0/A$. These arguments apply strictly to ionisation at sufficiently large distances, $R \gg D \equiv 2\rho_0$.

With reference to analytical applications, the most interesting aspect is the ionisation probability at small distances from the surface where there is maximum overlap between the incoming beam and the outgoing flow of ejected atoms. In this region a quantitative evaluation of the ion production rate is difficult because one needs to perform radial and angular integrations over basically unknown distributions. The results of this study clearly showed that an increase in beam size at a fixed beam current causes a pronounced reduction of the near-surface signal due to GPG ions. This observation cannot be discussed with reference to Eq. (11) which applies only to comparatively large distances. The situation encountered at small distances may, however, be discussed by considering a cylindrical volume $\pi\rho_0^2 L$ through which a constant flow of ejected gas atoms passes. The ionisation probability in this volume is given by Eq. (12), i.e., $\alpha^+ \propto \varphi_0 = \nu_0/\pi\rho_0^2$. Hence the ion production rate and the measured ion signal should decrease with increasing beam size as $1/\rho_0^2$. A test of this prediction is difficult because it requires a change of the beam size without changing the shape of the beam. This cannot be achieved by simply going from a focussed to a defocussed beam. In fact, the current density distribution in a defocussed beam is usually more uniform than in a focussed beam. A disadvantage of using a focussed beam is that the near-surface ionisation efficiency is relatively poor because a large fraction of the ejected gas atoms soon escapes radially from the region of high ionisation probability near the beam axis. The situation is much more favourable with a beam featuring a more uniform current density distribution. The results of Fig. 3 support this reasoning. By visual inspection of the beam size on a fluorescent screen, the diameter of the defocussed beam was three times larger than of the focussed beam. Hence one might have inspected the signals to differ by a factor of nine. The observed ratio was only 4.3. In other words, if the focussed beam would have had the same (normalised) shape as the defocussed beam, the near-surface signal would have been a factor of about two higher than measured.

These arguments appear to be of relevance when trying to understand the results reported by Ray et al. [9] who measured depth profiles of Ar and Kr implanted in semiconductors by gas-phase ionisation under O_2^+ and as $ArCs^+$ and $KrCs^+$ using Cs^+ bombardment. Unfortunately, the method of varying and determining the beam size was not specified. Using the quoted erosion rates and raster sizes in combination with known sputtering yields at the relevant impact angles [34], the beam currents must have ranged between 0.5 and 1 μA, the beam sizes $2\rho_0$ between 35 and 50 μm. In this size range accurate control of changes in size and shape is very difficult. Not surprisingly, the maximum yields I_m observed at depths corresponding to the peaks of the implantation distribution do not comply with the predictions of this study. Instead, the results compiled in Fig. 10(a) for GPG Kr^+ ions seem to suggest a dependence of the form $I_m \propto j^4$, much stronger than the dependence $I_m \propto j^2$ expected when changing the current density while keeping the beam shape constant. The results are compatible with the idea that the maximum-to-minimum ratio of the employed beam currents was 1.9 and the beam size was (almost) constant.

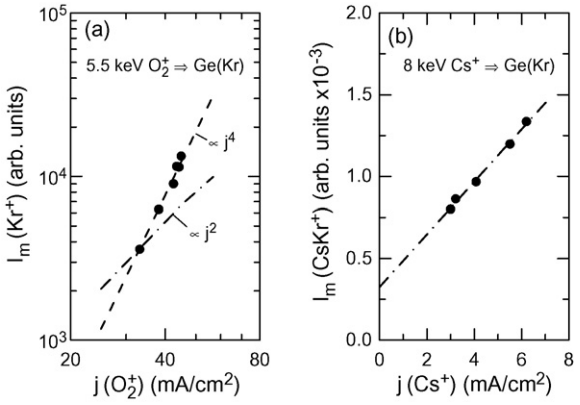

Fig. 10. Maximum yield of (a) GPG Kr^+ ions and (b) $KrCs^+$ secondary ions versus the estimated current density of (a) the O_2^+ and (b) the Cs^+ primary ion beam. Raw data from Ref. [9].

The problems encountered by the authors [9] when trying to evaluate current densities are also evident from Fig. 10(b). The results imply that the $KrCs^+$ signal depends on the Cs^+ current density, but with an offset independent of current density. There is no evidence in the literature for such a dependence. The experiments were presumably performed with different beam currents, but the beam size was not determined properly. In any case, the results provide further evidence that SIMS measurements aimed at identifying a possible dependence of the signal on the current density, as in the case of GPG ions, deserve extreme care before they should be considered meaningful.

One important result of the work of Ray et al. [9] was the finding that the maximum signals for Ar^+ and Kr^+ were independent of the matrix (Si, Ge and GaAs) in which the rare gas ions were implanted. This observation supports the idea that the ionisation probability of GPG rare gas ions does not depend significantly the state of excitation in which the atoms escape from the target or that the excitation state was independent of the target material. For polycrystalline samples the results of the present study suggest that the maximum achievable signal is determined by the angular distribution of microcrystals and presumably by the texture of the sample.

It is not yet clear whether one might gain peak intensity by using an energy analyser specifically designed for optimum transport of GPG ions. The critical question is how large the interaction length can made in units of the beam diameter before the loss of atoms due to escape from the interaction volume becomes more severe than the gain in ionisation probability. In any case, high beams currents in combination with small beam diameters will result in high ionisation probabilities.

5. Conclusion

This study has shown that the finer details of gas-phase ionisation of inert gases may be explored using a quadrupole-based mass spectrometer featuring a low extraction voltage in combination with a good energy resolution. The observed energy spectra are consistent with the idea that inert gas atoms released from solids escape with very low energies, on the order of 0.1 eV or less. The model developed for gas-phase ionisation by charge transfer provided the basis for quantifying, for the first time, two particularly important aspects of the process, (i) the dependence of the ion production rate on the beam current and/or the current density and (ii) on the distance from the surface. Somewhat unexpectedly, the results imply that ionisation events can be identified at distances as large as several millimetres. In order to perform spatially resolved studies it is necessary that the strength of the extraction field does not significantly exceed w_i/D, the ratio of the inherent resolution, w_i, of the energy analyser to the beam size D.

One of the problems encountered in the present and the previous work relates to the use of focussed beams with strongly non-uniform current density distributions. Hence a comparison of experimental results with the predictions of the model was only possible in terms of poorly defined mean current or flux densities. Rather convincing evidence was provided that gas atoms released from sputtered solids exhibit a strongly forward peaked angular distribution. Hence the gas-phase ionisation technique appears to be particularly useful for samples which become amorphised by ion bombardment. In the case of polycrystalline samples a significant fraction of the released gas atoms is lost from the ionisation volume due to oblique angles of emission. This aspect deserves further attention. Attempts should also be made to develop ion guns that provide higher beam current densities than currently available systems.

References

[1] J.-F. Hennequin, G. Blaise, G. Slodzian, C. R. Acad. Sci. Paris 268 (1969) 1507.
[2] M. Bernheim, G. Blaise, G. Slodzian, Int. J. Mass Spectrom. Ion Phys. 10 (1972–1973) 293.
[3] K. Wittmaack, Nucl. Instrum. Methods 132 (1976) 381.
[4] K. Wittmaack, in: A. Quayle (Ed.), Advances in Mass Spectrometry VIII, Heyden, London, 1980, p. 503.
[5] K. Wittmaack, Surf. Sci. 345 (1996) 110.
[6] R. Holland, G.W. Blackmore, Surf. Interf. Anal. 4 (1982) 174.
[7] R. Holland, G.W. Blackmore, Int. J. Mass Spectrom. Ion Phys. 46 (1983) 527.
[8] P. Williams, L.A. Streit, Nucl. Instrum. Methods Phys. Res. B 15 (1986) 159.
[9] M.A. Ray, J.E. Baker, C.M. Loxton, J.E. Greene, J. Vac. Sci. Technol. A 6 (1988) 44.
[10] P.A.W. van der Heide, J.B. Metson, D.L. Tui, W.M. Lau, Surf. Sci. 280 (1993) 208.
[11] R.G. Wilson, S.W. Novak, J. Appl. Phys. 69 (1991) 466.
[12] G. Slodzian, Phys. Scripta T6 (1983) 54.
[13] M.L. Yu, Nucl. Instrum. Methods Phys. Res. B 18 (1987) 542.
[14] M.L. Yu, N.D. Lang, Nucl. Instrum. Methods Phys. Res. B 14 (1986) 403.
[15] K. Wittmaack, Mat. Fys. Medd. Dan. Vid. 52 (2006) 465.
[16] R.G. Wilson, V.R. Deline, C.G. Hopkins, Appl. Phys. Lett. 41 (1982) 929.
[17] L. Desgranges, B. Pasquet, Nucl. Instrum. Methods Phys. Res. B 215 (2004) 545.
[18] K. Wittmaack, Vacuum 32 (1982) 65.
[19] H.-U. Gersch, K. Wittmaack, J. Vac. Sci. Technol. A 11 (1993) 125.
[20] G.N.A. van Veen, F.H.M. Sanders, J. Dieleman, A. van Veen, D.J. Oostra, A.E. de Vries, Phys. Rev. Lett. 57 (1986) 739.
[21] N. Menzel, K. Wittmaack, Nucl. Instrum. Methods Phys. Res. B 7/8 (1985) 366.
[22] K. Wittmaack, P. Blank, W. Wach, Rad. Effects 39 (1978) 81.
[23] B.Y. Tsaur, Z.L. Liau, J.W. Mayer, T.T. Sheng, J. Appl. Phys. 50 (1979) 3978.

[24] K. Wittmaack, M.G. Dowsett, J.B. Clegg, Int. J. Mass Spectrom. Ion Phys. 43 (1982) 31.
[25] U. Fano, W. Lichten, Phys. Rev. Lett. 14 (1965) 627.
[26] F.W. Saris, Physica 52 (1971) 290.
[27] R. Hegerberg, T. Stefánsson, M.T. Elford, J. Phys. B: Atom. Molec. Phys. 11 (1978) 133.
[28] H.B. Michaelson, J. Appl. Phys. 48 (1977) 4729.
[29] S.N. Schauer, P. Williams, Phys. Rev. B 46 (1992) 15452.
[30] K. Wittmaack, Int. J. Mass Spectrom. Ion Phys. 42 (1982) 43.
[31] K. Wittmaack, Appl. Phys. 12 (1977) 149.
[32] R.A. Haring, R. Pedrys, A. Haring, A.E. de Vries, Nucl. Instrum. Methods Phys. Res. B 4 (1984) 40.
[33] J. Tümpner, in: A. Benninghoven, A.M. Huber, H.W. Werner (Eds.), Secondary Ion Mass Spectrometry VI, J. Wiley & Sons, New York, 1988, p. 797.
[34] K. Wittmaack, Nucl. Instrum. Methods Phys. Res. 218 (1983) 307.